JOURNAL OF AIRCRAFT
Vol. 31, No. 2, March–April 1994

Supersonic Transport Wing Minimum Weight Design Integrating Aerodynamics and Structures

J.-F. M. Barthelemy*
NASA Langley Research Center, Hampton, Virginia 23681
G. A. Wrenn† and A. R. Dovi‡
Lockheed Engineering and Sciences Company, Hampton, Virginia 23666
P. G. Coen§
NASA Langley Research Center, Hampton, Virginia 23681
and
L. E. Hall¶
Unisys Corporation, Hampton, Virginia 23666

An approach is presented for determining the minimum weight design of aircraft wing models which takes into consideration aerodynamics-structure coupling when calculating both zeroth-order information needed for analysis and first-order information needed for optimization. When performing sensitivity analysis, coupling is accounted for by using a generalized sensitivity formulation. The results presented show that the aeroelastic effects are calculated properly and noticeably reduce constraint approximation errors. However, for the particular example selected, the error introduced by ignoring aeroelastic effects are not sufficient to significantly affect the convergence of the optimization process. Trade studies are reported that consider different structural materials, internal spar layouts, and panel buckling lengths. For the formulation, model, and materials used in this study, an advanced aluminum material produced the lightest design while satisfying the problem constraints. Also, shorter panel buckling lengths resulted in lower weights by permitting smaller panel thicknesses and generally, unloading the wing skins and loading the spar caps. Finally, straight spars required slightly lower wing weights than angled spars.

Nomenclature

Four different grids are used for reference of vector quantities: 1) the aerodynamic pressures and forces are calculated on a 15 × 15 grid overlaid over the aircraft planform; 2) the concentrated masses and inertia forces are found on an uneven inertia grid; 3) both pressure and inertia grids are combined on a total grid; and 4) constraints are calculated on 5 × 5 grids overlaid over each trapezoidal panel making up the aircraft configuration.

$\boldsymbol{A}$ = diagonal matrix containing reference areas on pressure grid
$\boldsymbol{b}_u, \boldsymbol{b}_v, \boldsymbol{b}_w$ = elastic displacement modes in x, y, and z directions
$\boldsymbol{f}_a^l$ = aerodynamic pressure loads, on pressure grid
$\boldsymbol{f}_i^l$ = inertia loads, on inertia grid
$\boldsymbol{f}_t^l$ = total point loads, on total grid
g_j = constraint function
$\boldsymbol{g}^l$ = vector of constraints
KS = Kresselmeier-Steinhauser envelope constraint, Eq. (2)
$\boldsymbol{P}^l$ = matrix of pressures due to elastic displacement modes, on pressure grid
$\boldsymbol{p}^l$ = vector of total pressures, on pressure grid
$\boldsymbol{p}_c^l$ = vector of pressures due to camber, on pressure grid
$\boldsymbol{p}_\alpha^l$ = vector of pressures due to a unit angle of attack, on pressure grid
$\boldsymbol{p}_o^l$ = vector of pressures due to rigid camber, on pressure grid
n^l = vertical load factor
$\boldsymbol{u}$ = vector of 1
u = polynomial approximation of elastic displacements
u^l, v^l, w^l = vectors of generalized displacements
w_e = aircraft empty weight
w_f^l = fuel weight
w_g^l = aircraft gross weight
$\boldsymbol{w}_e$ = vector of lumped empty weights
$\boldsymbol{w}_f^l$ = vector of lumped fuel weights
x = chordwise coordinate
x_{cg}^l = center of gravity longitudinal position, aircraft with fuel
x_{cge} = center of gravity longitudinal position, aircraft without fuel
x_{cgf}^l = fuel center of gravity longitudinal position
x_{cp}^l = center of pressure
$\boldsymbol{x}_p$ = vector of longitudinal positions of concentrated load application points
$\boldsymbol{x}_s$ = vector of independent structural design variables

Presented as Paper 92-2372 at the AIAA/ASME/ASCE/AHS/ASC 33rd Structures, Structural Dynamics, and Materials Conference, Dallas, TX, April 13–15, 1992; received June 9, 1992; revision received Dec. 16, 1992; accepted for publication Jan. 28, 1993.

*Senior Research Scientist, Aeroelastic Analysis and Optimization Branch, Structural Dynamics Division, M/S 246. Senior Member AIAA.
†Staff Engineer, Interdisciplinary Research Methods, 144 Research Drive. Member AIAA.
‡Supervisor, Interdisciplinary Research Methods, 144 Research Drive. Senior Member AIAA.
§Aerospace Engineer, Vehicle Integration Branch, Advanced Vehicle Division, M/S 412.
¶Programmer-Analyst; currently at the Computer Science Corporation, 3217A N. Armistead Ave., Hampton, VA 23666. Member AIAA.

y = spanwise coordinate
$\mathbf{y}_{as}$ = vector of dependent variables calculated by aerodynamics and used in structures
$\mathbf{y}_{sa}$ = vector of dependent variables calculated by structures and used in aerodynamics
$\mathbf{y}_{ss}$ = vector of dependent variables calculated by structures and not used anywhere else
α^l = trim angle-of-attack
ρ = user specified coefficient in the *KS* function, Eq. (2)

Superscripts
l = one of the flight conditions
T = transposed of a matrix or vector

Introduction

THIS article reports on a study to formally carry out the integration of aerodynamic and structural analyses in the minimum weight design of a supersonic transport aircraft wing. This is a necessary first step in carrying out the complete integration of aerodynamic, performance, and structural analyses in the optimization of the shape and structural design of a wing for optimum performance. The general approach to solve the latter problem has been discussed by Barthelemy et al.[1] and will not be repeated here. Instead, the focus is on the details of the formulation of the static aeroelastic problem, on the implementation of the optimization procedure, and also, on the latest technical results.

The capability to perform minimum weight structural design under static aeroelastic constraints has existed for a long time. In most applications, however, the aeroelastic coupling is only accounted for while performing system analysis, i.e., while computing zeroth-order information, like loads, displacements, stresses, and strains. Specifically, the coupling effect is ignored while performing system sensitivity analysis, i.e., calculating first-order gradient information necessary for optimization. In this article, the coupling is explicitly accounted for in both analysis and sensitivity analysis. The tool used to explicitly account for the coupling between the disciplines is the "generalized sensitivity equations" discussed at length by Sobieski.[2]

This study is part of high-speed aircraft integration research (HiSAIR), a research effort at the NASA Langley Research Center. As discussed by Dollyhigh and Sobieski,[3] HiSAIR is a research program addressing the multidisciplinary nature of aircraft analysis and design. Many disciplinary organizations at NASA Langley participate in this program which focuses on high-speed civil transport aircraft. Coen et al.[4] give a thorough activity-by-activity review of the status of HiSAIR. The current vehicle focus for HiSAIR is a civil transport aircraft designed to carry 252 passengers for 6500 n.mi. at a Mach number of 2.4 at a midcruise altitude of 63,000 ft.

This article begins with a discussion of the problem formulation, reviewing the specifics of the structural, aerodynamic, and aeroelastic analyses and sensitivity analyses. Then the optimization procedure is discussed. Finally, a section describes current results; it includes a discussion of the trade studies that consider different materials and internal spar layouts.

Problem Formulation

Structural Analysis and Modeling

Structural analysis is performed using the equivalent laminated plate formulation implemented in program ELAPS,[5,6] a code based on the Rayleigh-Ritz method. It can model wing skin as well as rib and spar caps. In ELAPS, the analysis process begins with a wing described by planform geometry, thickness, camber, and material information, and modeled by several trapezoidal plates. ELAPS then proceeds by assuming that the three displacement fields for the wing can be represented by polynomials in the x and y coordinates. For each flight condition

$$u^l(x, y) = \mathbf{b}_u^T(x, y)\mathbf{u}^l$$
$$v^l(x, y) = \mathbf{b}_v^T(x, y)\mathbf{v}^l \quad (1)$$
$$w^l(x, y) = \mathbf{b}_w^T(x, y)\mathbf{w}^l$$

where the entries of vectors $\mathbf{b}_u$, $\mathbf{b}_v$, $\mathbf{b}_w$ are products of the type $x^n y^m$.

Figures 1 and 2 depict the aircraft models considered in this study; they differ by whether the spars are straight and swept or cranked so as to be orthogonal to the fuselage axis. Each model is made of 11 separate plates, one of which (plate 11) constitutes a model of the fuselage scaled to match known fuselage weight data. The model has 4 spars and 10 ribs whose caps can be modeled by ELAPS. The boundary conditions specify symmetry of the displacements about the centerline. In addition, the model is supported in pitch by two springs; however, as explained later, the aerodynamic and inertia loads are balanced in each flight condition, so that the reactions in the springs are zero, or nearly so. The wing skins are sandwich panels with a 0.75-in.-thick honeycomb core.

Earlier comparisons between finite element and ELAPS results for similar models have pointed to the difficulty to capture stresses in models with complex planform, thickness, and camber distributions adequately. While it would be desirable in such cases to use higher-order polynomials, the current implementation of ELAPS, based on simple polynomial displacements, does not permit it. Therefore, to obtain reasonable stress distributions, the current model neglects the camber of the wing and calculates stresses, assuming a symmetric airfoil. The highest power appearing in the elastic displacement modes are x^4y^5 for $\mathbf{u}^l$ and $\mathbf{v}^l$, and x^4y^6 for $\mathbf{w}^l$. This results in 25 generalized degrees of freedom (DOF) for displacements $\mathbf{u}^l$ and $\mathbf{v}^l$, and 30 DOF for displacement $\mathbf{w}^l$. The whole model therefore has 80 DOF.

Given a selection of $\mathbf{b}$, and point forces $\mathbf{f}_i^l$, ELAPS calculates the generalized displacements. From those displacements, it finds stresses and strains in the wing covers. These are evaluated on upper and lower wing skins, on a 5 × 5 grid on each individual plate. Conventional constraints are then evaluated for the three plane strains, the von Mises stress, as well as orthotropic panel buckling. The buckling constraint is an orthotropic buckling equation given for a simply supported plate by Sobieski[7]; the critical shear load of an infinite length strip is taken from the DOD/NASA *Advanced Composite Design Guide*.[8]

ELAPS also finds strains and stresses evaluated at five equally spaced stations on each cap. Stress and strain constraints are

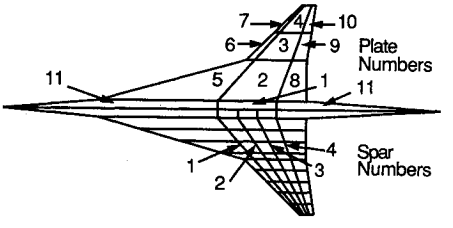

Fig. 1 Swept spar model definition, plate and spar numbering.

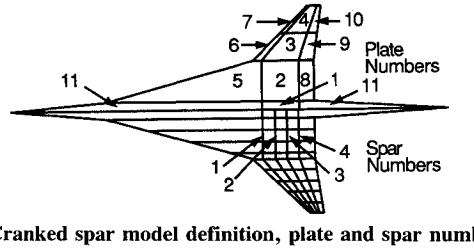

Fig. 2 Cranked spar model definition, plate and spar numbering.

calculated at those stations. Finally, ELAPS also evaluates the structural weight.

Only plates 1–10 are retained when calculating constraints because it is felt that the fuselage stresses are not representative of actual stresses. This leaves 500 of the plate constraints and 460 of the cap constraints. This makes for a very large number of constraints for the optimizer to handle. To reduce that number, an envelope function developed by Kresselmeier and Steinhauser[9] is used to combine all constraints of the same type for a given flight condition; this leaves five plate envelope constraints and two cap envelope constraints for each flight condition. For a set of individual g_j, the envelope constraint is defined by

$$KS = \frac{1}{\rho} \ln \left[\sum_j \exp(\rho g_j) \right] \tag{2}$$

Parameter ρ must be carefully selected,[10] the larger the value of ρ, the closer the envelope is to the initial constraints boundaries. On the other hand, excessively large values of ρ cause the envelope to have nearly discontinuous gradients.

The wing panel face sheet thicknesses at each panel corner are taken as design variables, and the skin thickness is assumed to vary linearly between the corners. The spar cap cross-sectional areas at the plate boundaries are design variables and the cross-sectional areas vary linearly between plate boundaries. Finally, the rib cap cross-sectional areas are variables, and each rib cross-sectional area is constant between leading-edge and trailing-edge spars. The upper and lower wing covers are identical. There is a total of 44 design variables describing the model, they are contained in $\boldsymbol{x}_s$.

Aerodynamic Analysis and Modeling

Aerodynamic analysis is performed with the WINGDES computer program from Carlson and Walkey.[11] WINGDES computes subsonic and supersonic pressure distributions on a 15 × 15 grid overlaid on the aircraft planform. In both modes, it uses a lifting surface formulation. For each flight condition, the linearity of pressure distributions enables p_α^l and p_c^l. The pressue due to camber is due to the rigid camber (and twist) built into the wing, as well as to the elastic deformations resulting from the airloads. The pressure due the transverse displacement $w^l(x, y) = \boldsymbol{b}_w^T(x, y)\boldsymbol{w}^l$ can be found by superposition as

$$\boldsymbol{p}_e^l = \boldsymbol{P}^{lT}\boldsymbol{w}^l \tag{3}$$

where $\boldsymbol{P}^l$ is a matrix, each column of which is a vector of pressures due to one of the transverse displacement modes. It must be noted that vectors $\boldsymbol{p}_\alpha^l$, $\boldsymbol{p}_o^l$, and matrix $\boldsymbol{P}^l$, are fixed for any given flight condition and wing planform.

Integrated Static Aeroelastic Analysis

The object of integrated aeroelastic analysis is to find the airloads and resulting elastic wing displacements which result in a trimmed aircraft in the various flight conditions. Those conditions are summarized in Table 1. Trimming is effected by selecting the angle of attack of flight that balances the total vertical load on the aircraft, as well as the fuel distribution that balances the pitching moment. Since the aircraft is tailless, the latter condition requires that the aircraft c.p. and c.g. are collocated.

The given input geometry corresponds to the cruise condition ($l = 1$). The jig shape is obtained by removing cruise elastic displacements $\boldsymbol{w}^1$ from the input camber. In any off-cruise flight condition, the elastic deformations from cruise shape are given by $\boldsymbol{w}^l - \boldsymbol{w}^1$.

The total pressure due to camber can now be written

$$\boldsymbol{p}_c^l = \boldsymbol{p}_o^l + \boldsymbol{P}^{lT}(\boldsymbol{w}^l - \boldsymbol{w}^1) \tag{4}$$

so that the total aerodynamic pressure, including elastic effects is given by

$$\boldsymbol{p}^l = \boldsymbol{p}_c^l + \alpha^l \boldsymbol{p}_\alpha^l \tag{5}$$

and the total aerodynamic forces are then

$$\boldsymbol{f}_a^l = \boldsymbol{A}\boldsymbol{p}^l \tag{6}$$

The vertical force equilibrium equation is used to find the trim angle of attack. Neglecting rotary inertias

$$n^l w_g^l = \boldsymbol{u}^T \boldsymbol{f}_a^l = \boldsymbol{u}^T \boldsymbol{A}(\boldsymbol{p}_c^l + \alpha^l \boldsymbol{p}_a^l) \tag{7}$$

The aircraft is trimmed in pitch by moving fuel among the different tanks so that the c.g. coincides with the c.p. $x_{\text{cg}}^l = x_{\text{cp}}^l$. The c.p. location is given by

$$x_{\text{cp}}^l = \frac{\boldsymbol{f}_a^{lT}\boldsymbol{x}_p}{\boldsymbol{f}_a^{lT}\boldsymbol{u}} \tag{8}$$

The total c.g. location is given by

$$x_{\text{cg}}^l w_g^l = x_{\text{cge}} w_e + x_{\text{cgf}}^l w_f^l \tag{9}$$

Pitch equilibrium determines a target position for the fuel c.g. that is given by

$$x_{\text{cgf}}^l = \frac{x_{\text{cg}}^l w_g^l - x_{\text{cge}} w_e}{w_f^l} \tag{10}$$

To obtain that target position, the existing fuel is distributed in the tanks, starting from those closest to the target position, so that their moment with respect to that position remains exactly zero. With the current tank layout, this process has proven generally feasible and extremely fast. It must be noted that while this approach is generally correct for straight and level flight conditions, it is quite approximate for pull ups since 1) rotary inertias are neglected and 2) it would not be possible to move fuel fast enough to trim the aircraft in such a condition.

The inertia loads are given on the inertia grid, they become

$$\boldsymbol{f}_i^l = n^l(\boldsymbol{w}_e + \boldsymbol{w}_f^l) \tag{11}$$

Table 1 Flight conditions description

Load case	Load factor	Mach number	Altitude, ft	Dynamic pressure, lb/ft²	Fuel weight, lb
1) Midcruise	1.0	2.4	63,175	535	85,544
2) Transonic climb	1.0	1.2	29,670	644	167,016
3) Reserve cruise	1.0	0.9	42,480	199	18,446
4) High-speed pull up	2.5	2.4	56,949	723	149,830
5) Low-speed pull up	2.5	0.6	10,000	367	174,185

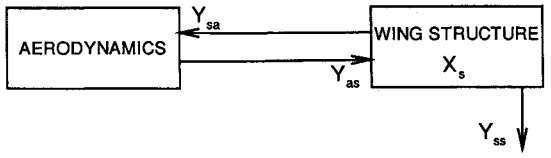

Fig. 3 Problem functional description, independent and dependent variables definition.

The total vector of concentrated forces becomes, by concatenation

$$f_i^I = (f_i^{IT}, f_a^{IT})^T \tag{12}$$

For given flight conditions and aircraft planform and camber distributions, the analysis begins with generation of vectors p_α^I, p_o^I, and matrix P^I. Then, for each flight condition, an iterative loop follows that first finds the pressure due to camber, then the trimmed angle of attack and fuel distribution, as well as the total pressure distribution and the total loads on the wing. Structural analysis is performed to calculate a new elastic camber and the process is restarted. The iterative loop continues until convergence.

This procedure was validated by comparing its predictions with those from the TSO program[12] for a simple trapezoidal swept wing trimmed in angle of attack only. In a 2.5g pull up at a Mach number of 0.45, the approaches yielded differences of 5% in rigid and elastic trim angles of attack and 3% in wing tip displacement.

Integrated Aeroelastic Sensitivity Analysis

The formulation outlined above shows coupling of aerodynamic and structural disciplines. Integrated sensitivity analysis can be applied to obtain total sensitivity derivatives that account for the coupling. This requires clearly identifying the disciplines interacting in the coupled system and delineating the boundaries between those disciplines.

The coupled set of equations for the aeroelastic system described above can be written functionally as follows:

$$\begin{aligned} y_{as} &= y_{as}(y_{sa}) \\ y_{sa} &= y_{sa}(x_s, y_{as}) \\ y_{ss} &= y_{ss}(x_s, y_{as}) \end{aligned} \tag{13}$$

Equation (13) identifies the relationships between the outputs of a discipline and its inputs. These inputs may be either independent or dependent variables calculated by another discipline. In this notation, the first subscript identifies the discipline where the dependent variable is calculated, the second subscript, where it is used. When the subscript is repeated, the dependent variable is calculated, but not used in any other discipline analysis; it is used in the design process. Figure 3 gives a graphic description of the problem, identifying the disciplines as well as the independent and dependent variables.

Vector y_{as} contains the dependent variables calculated in the aerodynamic discipline and needed in the structural discipline for calculation of displacements, strains, and stresses. In principle, this would include vectors of aerodynamic pressures in the different flight conditions. However, because of the linear representation retained for the wing pressure, and of the fact that vectors p_α^I, p_o^I, and matrix P^I remain constant throughout the design, this information is limited to the amplitudes of the pressure modes in Eq. (4), i.e., the vectors of generalized displacements measured with respect to cruise shape:

$$y_{as} = [(w^2 - w^1)^T, (w^3 - w^1)^T, (w^4 - w^1)^T, (w^5 - w^1)^T]^T \tag{14}$$

Vector y_{sa} contains the dependent variables calculated in the structural discipline and needed in the aerodynamic discipline for calculation of pressures. This includes the generalized displacements in the different flight conditions:

$$y_{sa} = (w^{1T}, w^{2T}, w^{3T}, w^{4T}, w^{5T})^T \tag{15}$$

Finally, y_{ss} contains the aircraft gross weight at cruise and the envelope constraints in each of the load cases:

$$y_{ss} = (w_g^1, g^{1T}, g^{2T}, g^{3T}, g^{4T}, g^{5T})^T \tag{16}$$

The generalized sensitivity equations read

$$\begin{bmatrix} I & -\frac{\partial y_{as}}{\partial y_{sa}} & 0 \\ -\frac{\partial y_{sa}}{\partial y_{as}} & I & 0 \\ -\frac{\partial y_{ss}}{\partial y_{as}} & 0 & I \end{bmatrix} \begin{bmatrix} \frac{dy_{as}}{dx_s} \\ \frac{dy_{sa}}{dx_s} \\ \frac{dy_{ss}}{dx_s} \end{bmatrix} = \begin{bmatrix} 0 \\ \frac{\partial y_{sa}}{\partial x_s} \\ \frac{\partial y_{ss}}{\partial x_s} \end{bmatrix} \tag{17}$$

This equation gives the sensitivity derivatives of the dependent variables accounting for the coupling between the disciplines: the *total derivatives* $[(\mathrm{d}(.)/\mathrm{d}(.)]$ as a function of the sensitivity derivatives ignoring the coupling between the disciplines: the *partial derivatives* $[\partial(.)/\partial(.)]$.

For example, $\partial y_{as}/\partial y_{sa}$ is the matrix of derivatives of the amplitudes of the pressure modes with respect to the amplitudes of the displacement modes; using Eqs. (14) and (15), it is quite simple to calculate and is given by

$$\frac{\partial y_{as}}{\partial y_{sa}} = \begin{bmatrix} -I & I & 0 & 0 & 0 \\ -I & 0 & I & 0 & 0 \\ -I & 0 & 0 & I & 0 \\ -I & 0 & 0 & 0 & I \end{bmatrix} \tag{18}$$

Also, $\partial y_{sa}/\partial y_{as}$ and $\partial y_{ss}/\partial y_{as}$ are matrices of derivatives of the elastic deformations, and the weight and stresses, respectively, with respect to the amplitudes of the pressure modes. Finally, $\partial y_{sa}/\partial x_s$, and $\partial y_{ss}/\partial x_s$ are matrices of derivatives of the elastic deformations, and the weight and stresses, respectively, with respect to the structural design variables. The last four derivative matrices are calculated by forward finite difference. In this application, this detailed formulation permits one to account for elastic load redistribution while calculating the gradients of the dependent variables, including the constraints.

There is a certain degree of arbitrariness in identifying the disciplines involved and in deciding where the boundary lines have to be drawn. In fact, there is no specific requirement that the calculations belonging to a given discipline be confined to a single block in the decomposition. Rather, each block can be thought of as a computational module performing a set of related calculations. Each classical discipline can then comprise several blocks. It turns out that there can be several valid decompositions of the problem. The elements to take into account when identifying the blocks include 1) what are the natural computational boundaries (it is impractical to define a boundary in the middle of a computer program); 2) what are the modules for which partial derivatives are already available or easy to obtain; and 3) what are the dependent variables for which total sensitivity information is required.

For example, in this problem one could have added a third discipline dealing with the balance of the aircraft. This would have added to the complexity of the decomposition, but would have generated more information, including the sensitivity of the aircraft trim angle of attack and c.g. position to changes in the design variables.

Table 2 Summary of final designs, all-titanium wing, swept spars

Buckling length, ft	3.0	2.5	2.0
Structural weight, lb	33,058	26,525	24,698
Active variable numbers			
Plates	3, 4, 5, 6, 7, 8	6, 7	6, 7
Spars		25, 29	24, 25, 28, 29
Active constraints			
Plates	b^5	v^2, b^5	v^2, v^5, (xy^2)
Spars			(s^2), (s^5)

Superscripts indicate load case.

Table 3 Summary of final designs, all-aluminum wing, swept spars

Buckling length, ft	3.0	2.5
Structural weight, lb	25,791	23,295
Active variable numbers		
Plates	4, 6, 7, 8, 9	6, 7, 8
Spars	25, 29	21, 24, 25, 28, 29, 32
Active constraints		
Plates	v^2, b^5	v^2, xy^5
Spars		(s^2)

Superscripts indicate load case.

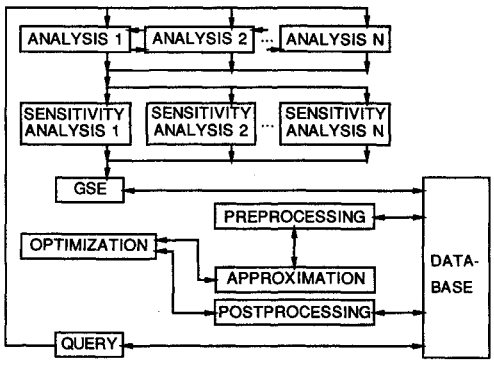

Fig. 4 Integrated design system.

Optimization

Figure 4 presents a graphic description of the generic optimization capability developed in this study. It is a SUN engineering workstation based system currently implemented to handle 5 disciplines with up to 100 independent variables and 500 dependent variables. The system is designed to provide for user intervention at any point in the design process. Alternately, the system can operate completely automatically. It proceeds in design cycles, each requiring full analysis and sensitivity analysis of the problem. Within each cycle, it is possible to change such things as the type of problem approximation, the type of optimization algorithm used, the combination of dependent and independent variables optimized, and the move limits for approximations. Each change of one or several of these parameters produces a different design alternative.

The system is built around the commercial package OPTDES[13] which offers several optimization algorithms. Those used in this study are linear programming, sequential linear programming, method of centers, generalized reduced gradients, and sequential quadratic programming. Since analyses and sensitivity analyses are quite expensive, OPTDES optimizes a sequence of approximations to the actual design problem. These approximations are all based on zeroth- and first-order information of the dependent variables and include linear, reciprocal, convex, and the two-point approximation of Fadel et al.[14] For the results generated in this article, the combination of two-point approximation and sequential linear programming proved the best.

Because of the use of approximations, move limits must be imposed to guarantee convergence of the optimization process. However, move limits may prevent design progress from an infeasible starting point. To avoid this problem, a constraint relaxation procedure similar to that discussed by Barthelemy and Riley[10] is implemented.

To provide an audit trail for the design process and allow for restart from any design cycle, critical optimization information is stored primarily in the relational information manager (RIM[15]), a commercial relational data base management system. Cycle information retained includes initial values and upper and lower bounds on the independent and dependent variables. Because of its potential size, cycle gradient information is kept in conventional file format. Design alternative information retained includes final independent and dependent variables for each alternative design within each cycle.

Each design cycle begins with system analysis and subsystem sensitivity analysis. This step can be conducted with any existing analysis package on any computer or distributed system of computers. Each discipline produces one file containing its own analysis and sensitivity analysis information. This information is then processed to produce the generalized sensitivity equations [(GSE), Eq. (17)], and relevant data is stored in the RIM data base and the gradient files. Once optimization is completed, the user may interactively query the data base and track graphically or in tabular output any combination of independent or dependent variables. The user may also gauge the accuracy of the approximations selected by comparing analysis results predicted with those obtained after reanalysis, and then decide to produce more design alternatives within the current cycle or to initiate a new cycle using as the starting design any of the design alternatives generated previously.

Results

Optimization Results

The procedure described in this article was used to find the minimum weight design of models with two different spar layouts, two different materials, and three different panel buckling lengths. In changing the buckling length, however, the weight of the spar and rib webs was assumed to remain constant. Tables 2–5 give summary results for optimization. In these tables, the structural weight includes wing skins and rib and spar caps for both covers of one wing. The active variables are those not locked against their lower bounds; lower bounds are set at 0.004 ft for the skin thicknesses, and 0.005 ft^2 for the cap cross-sectional areas. For the plates, the constraints are identified as v^l for von Mises, b^l for buckling, x^l for chordwise strain, y^l for spanwise strain, and xy^l for shear strain. For the caps, e^l is used for strain and s^l is used for stress. The constraints are written to range between -1.0 and 0.0 when satisfied. In the tables, the constraints are identified as active if between -0.02 and 0.0, and as nearly active (as indicated by parentheses) if between -0.1 and -0.02.

The active thickness variables are the thicknesses at the corners of the plates corresponding to the wing box (Figs. 1 and 2), i.e., plates 2 (variable number 3–6), 3 (5–8), and 4 (7–9). For the swept spars, the active variables are for spars 2 (24, 28, and 32) and 3 (21, 25, and 29); for the cranked spar case, spar 1 variables (19 and 23) become active also. Rib cap variables never stay active at the optimum.

Table 4 Summary of final designs, all-titanium, cranked spars

Buckling length, ft	3.0	2.5	2.0
Structural weight, lb	34,931	28,947	25,130
Active variable numbers			
Plates	5, 6, 7, 8, 9	5, 6, 7, 8, 9	5, 6, 7
Spars	26	25, 28	19, 23, 24, 28
Active constraints			
Plates	v^2, b^5, (xy^2)	v^2, b^5, (xy^2)	v^2, v^5, (y^5), (xy^2)
Spars			s^5, e^5

Superscripts indicate load case.

Table 5 Summary of final designs, all-aluminum, cranked spars

Buckling length, ft	3.0	2.5	2.0
Structural weight, lb	28,391	24,235	22,779
Active variable numbers			
Plates	5, 6, 7, 8	5, 6, 7, 8	5, 6, 7, 8
Spars	25, 28, 29	19, 25, 28, 29	25, 28, 29
Active constraints			
Plates	v^2, b^5, (xy^2)	v^2, b^5, (xy^2), s^5	v^2, (y^5), (xy^2)
Spars			(s^2), s^5, (e^5)

Superscripts indicate load case.

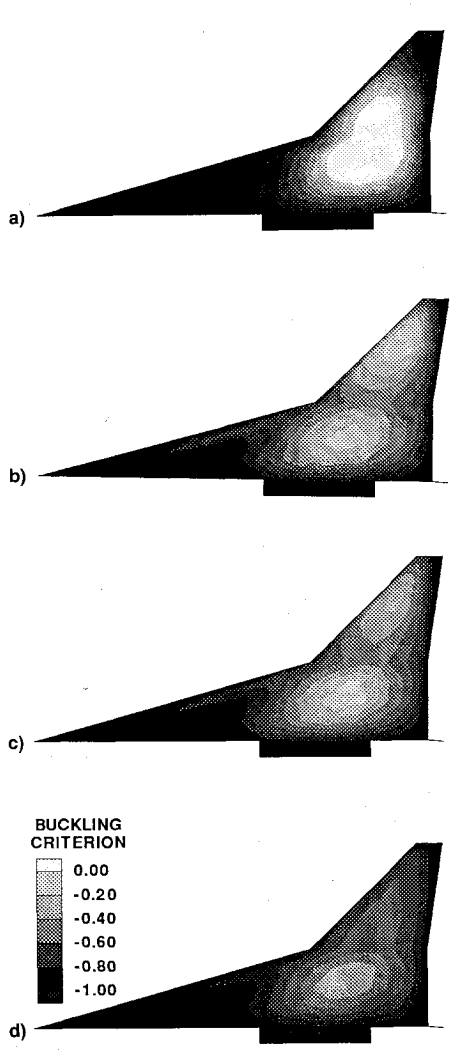

Fig. 5 Effect of panel buckling length on buckling criterion, upper skin, flight condition 5, all-titanium swept spar model: a) initial design, b) panel buckling length 3 ft, c) panel buckling length 2.5 ft, and d) panel buckling length 2 ft.

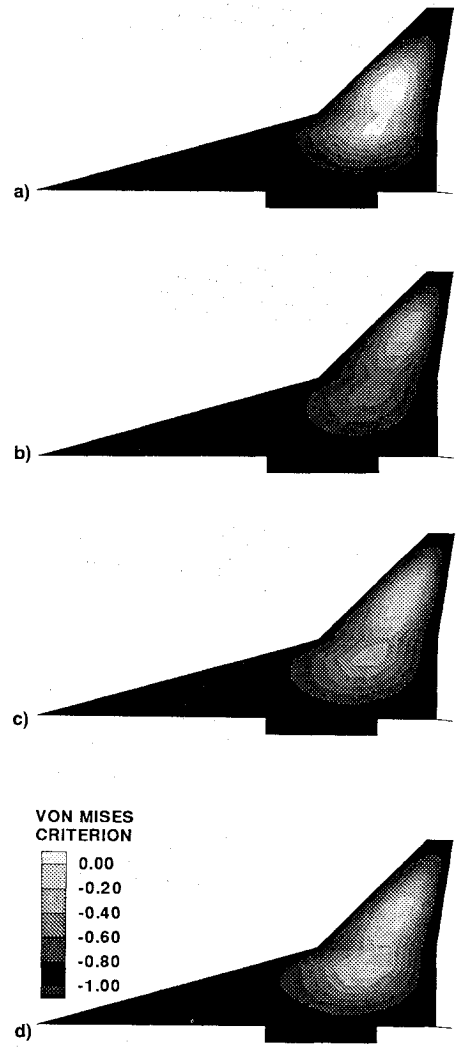

Fig. 6 Effect of panel buckling length on von Mises criterion, upper skin, flight condition 2, all-titanium swept spar model: a) initial design, b) panel buckling length 3 ft, c) panel buckling length 2.5 ft, and d) panel buckling length 2 ft.

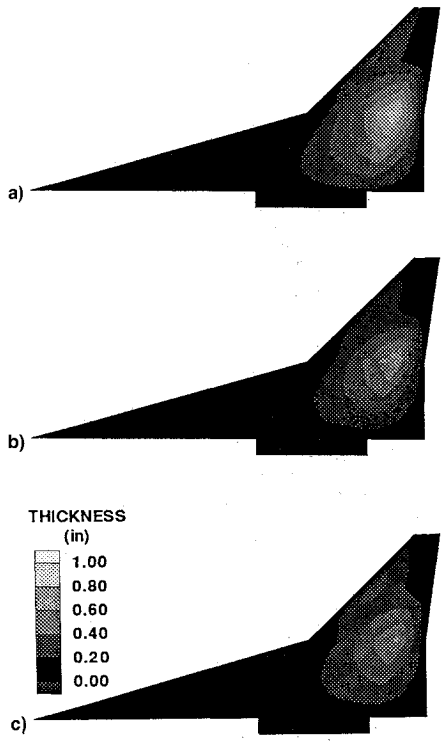

Fig. 7 Effect of panel buckling length on optimum skin thickness distribution, all-titanium swept spar model: a) panel buckling length 3 ft, b) panel buckling length 2.5 ft, and c) panel buckling length 2 ft.

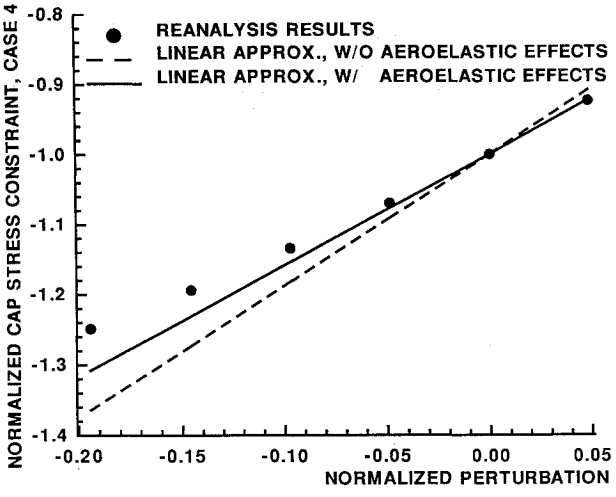

Fig. 8 Cap stress envelope constraint for high-speed pull up, all titanium swept spar design, 3-ft panel buckling length.

For each material and spar layout combination, the same trend develops with panel buckling length. The optimum design with the largest panel length is designed primarily by the buckling constraint in the low-speed pull up; notably no cap constraint is active and few cap variables are active. As the panel buckling length is decreased, buckling criticality decreases, thinner skins can be used and the loads are transferred to the spars. In the process, more cap variables and constraints become critical. This trend is a consequence of the facts that 1) spars and skins use the same material, and 2) because of the geometrical layout of the wing sections and of the definition of skin thickness variables, the spars offer more bending resistance for a given amount of structural weight. Therefore, if panel buckling is not an issue, it is more efficient to put the material in the spar caps.

Figures 5–7 demonstrate the trend graphically for the all-titanium design with swept spars. Figure 5 traces the buckling constraint in flight condition 5, the low-speed symmetric pull up. At the starting point, the constraint is violated on both the inboard and outboard sections. The 3-ft buckling length optimum design has the buckling constraint active on both the inboard and the outboard wing sections. As the buckling length is reduced, the constraint remains only active on the inboard section of the wing and then becomes inactive for a 2-ft buckling length. In contrast, Fig. 6 traces the von Mises criterion in flight condition 2, the transonic climb. Initially violated in the outboard section of the wing, the constraint is satisfied at the largest buckling length, and becomes active or nearly active for both inboard and outboard panels at the smallest buckling length.

Figure 7 shows the various optimum thickness distributions. Each has a maximum at the break between the inboard and outboard wing sections, over the trailing-edge spar. The maximum thickness decreases noticeably with the buckling length. While none of the active constraints are ever located at the wing break, the fact that the maximum thickness occurs at that location is directly related to the definition of skin thickness variables and skin thickness variation which guarantees a maximum thickness at a plate corner. Since the active constraints peak either in the inboard wing section or the outboard wing section, it is logical that the maximum thickness occurs at the break section, which defines the boundary between plates 2 and 3.

Additional comparison of Tables 2–5 shows the swept spar designs to be very slightly lighter than the cranked spar ones. This is because cranked spars pass through a thinner section of the wing, and are thus less efficient in bending. The advanced aluminum designs are lighter than the titanium ones, more so for the buckling dominated case (larger panel sizes); this is a direct consequence of the better specific stiffness of aluminum.

Optimization for given material, spar layout, and buckling length proceeded with between 20–50 cycles per design, each cycle lasting 1 h and 40 min on a combination of one IRIS and two SUN engineering workstations. The longest runs were required with the largest buckling length where buckling was an active constraint. As shown on Fig. 5, two different plates have critical or near-critical individual buckling constraints in that case. The envelope constraint combining the individual buckling constraints in a single constraint for optimization [Eq. (2)] exhibits a quickly-varying, nearly discontinuous gradient and oscillates between two designs, each dominated by one of the individual buckling constraints. To alleviate the problem, optimization was started with a low value of ρ, which was eventually increased to obtain sufficient accuracy. In the problems described here, ρ ranged from an initial value of 10 to a final value of 100. At the same time move limits starting at 20% and ending at 5% were used to maintain the quality of the approximations.

Sensitivity Analysis and Approximations Validation

It remains to demonstrate the validity and usefulness of including aeroelastic effects when calculating gradients. Figure 8 compares linear approximations with and without aeroelastic effects included in the gradient calculations for the cap stress constraint in the high-speed pull up. The reanalyses were performed for six designs located on a straight line between the cycle 1 and cycle 3 designs of the all-titanium model with swept spars and 3-ft buckling length. It is shown that including the aeroelastic effects noticeably improves the quality of the approximations, reducing the error in the slope of the approximation by about a factor of 4. Figure 9 compares the quality of the various approximations available in this study for the envelope buckling constraint in the same flight condition. It shows the linear approximation to be of lesser quality, while all three other approximations are comparable.

The effect of accounting for aeroelasticity on the rate of convergence of optimization is shown on Fig. 10 where the all-titanium, swept spar design is rerun. As can be seen, there is no clear benefit on convergence of including these effects. Both optimizations converge to essentially the same design, the final weights being within 300 lb. This is consistent with the fact that studies show that this model does not exhibit

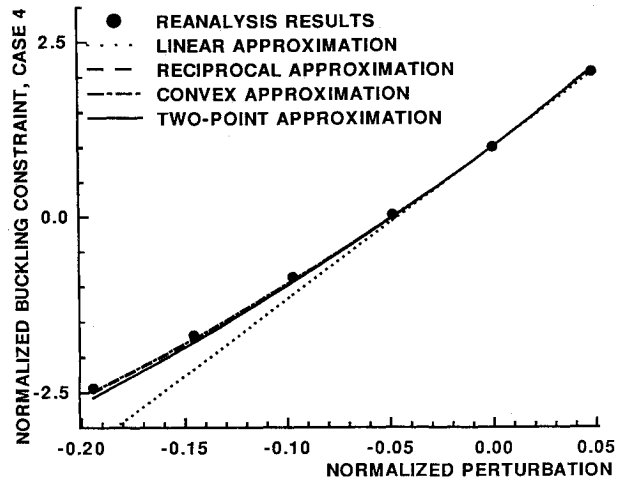

Fig. 9 Panel buckling envelope constraint for high-speed pull-up, all titanium swept spar design, 3-ft panel buckling length.

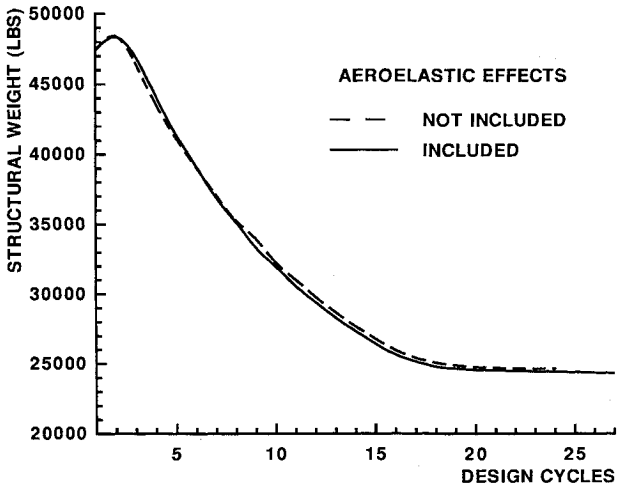

Fig. 10 Optimization convergence, all titanium swept spar design, 2-ft panel length.

radical aeroelastic load redistribution effects, particularly in flight conditions 2 and 5, which are critical in this design exercise. So, while including the aeroelastic effects improves the quality of the gradients and of the resulting approximations, the error introduced by neglecting these effects is not sufficient to alter the overall performance of the optimization algorithm. For this design this indicates that some simplifications can be made in the formulation and that the $\partial y_{as}/\partial y_{sa}$, $\partial y_{sa}/\partial y_{as}$, $\partial y_{ss}/\partial y_{as}$, $\partial y_{sa}/\partial x_s$ derivatives [Eq. (17)] need not be calculated. It must be noted, however, that this conclusion is problem-dependent and may not be applicable to other design problems, other level of analysis detail, or even other flight conditions.

Concluding Remarks

The results discussed in this article show that the aeroelastic effects on sensitivity information are calculated properly by the generalized sensitivity approach. In addition, accounting for these effects reduces noticeably approximation errors. However, for the particular example selected, the errors introduced by ignoring the aeroelastic effects are not sufficient to significantly affect the convergence of the optimization or the final solution.

Although the optimization procedure generally performs satisfactorily, oscillations occasionally appear when two of the same individual constraints are nearly active simultaneously for the same flight condition. In this case, envelope constraint gradients are nearly discontinuous and convergence is noticeably slowed. This problem is alleviated by adjusting the envelope function. At the beginning of optimization, the envelope is kept further away from the boundaries, thereby maintaining smooth gradients; as the optimum is neared, the envelope is brought closer to the original constraint boundaries.

Results are given that consider different structural materials, internal spar layouts, and panel buckling lengths. For the formulation, model, and materials used in this study, an advanced aluminum material generated the lightest design while satisfying the problem constraints. Also, lower panel buckling lengths resulted in lower weights by permitting lower panel thicknesses, and generally, unloading the wing skins and loading up the spar caps. Finally, swept spars generated slightly lighter design than cranked spars.

Table A1 Material properties and allowables

Material	Titanium	Advanced aluminum
E, psi	16.0×10^6	12.0×10^6
G, psi	6.0×10^6	4.78×10^6
ν	0.332	0.318
ρ, pci	0.163	0.105
$\sigma_x = \sigma_y$, yield, psi	$\pm 91.8 \times 10^3$	$\pm 61.5 \times 10^3$
σ_{xy}, yield, psi	$\pm 34.5 \times 10^3$	$\pm 23.3 \times 10^3$
$\varepsilon_x = \varepsilon_y$, yield	$\pm 5.74 \times 10^{-3}$	$\pm 5.13 \times 10^{-3}$
ε_{xy}, yield	$\pm 5.74 \times 10^{-3}$	$\pm 4.82 \times 10^{-3}$
$\sigma_x = \sigma_y$, fatigue, psi	$\pm 25.0 \times 10^3$	$\pm 15.0 \times 10^3$
σ_{xy}, fatigue, psi	$\pm 9.38 \times 10^3$	$\pm 5.69 \times 10^3$
$\varepsilon_x = \varepsilon_y$, fatigue	$\pm 1.56 \times 10^{-3}$	$\pm 1.25 \times 10^{-3}$
ε_{xy}, fatigue	$\pm 1.56 \times 10^{-3}$	$\pm 1.19 \times 10^{-3}$

Table A2 Safety factors used in the various constraints

Load cases	1, 2, 3	4, 5
Stress, strain	1.00	1.50
Buckling	1.50	2.25

Appendix: Material Properties, Allowables, and Safety Factors

Table A1 gives the material properties and allowables used in this study. Fatigue allowables were used in the first three flight conditions. Table A2 shows the safety factors selected in this problem. In general, a factor of 1.5 is used in the high-g load conditions. For the 1g flight conditions, where allowables are knocked down significantly to prevent fatigue of the material, a factor of 1.0 is used. For the buckling conditions, an additional safety factor of 1.5 is used.

References

[1]Barthelemy, J.-F. M., Coen, P. G., Wrenn, G. A., Riley, M. F., Dovi, A. R., and Hall, L. E., "Application of Multidisciplinary Optimization Methods to the Design of a Supersonic Transport," NASA TM-104073, March 1991.

[2]Sobieszczanski-Sobieski, J., "On the Sensitivity of Complex Internally Coupled Systems," *AIAA Journal*, Vol. 28, No. 1, 1990, pp. 153–160.

[3]Dollyhigh, S. M., and Sobieszczanski-Sobieski, J., "Recent Experiences with Multidisciplinary Analysis and Optimization in Advanced Aircraft Design," *Proceedings of III Air Force/NASA Symposium on Recent Advances in Multidisciplinary Analysis and Optimization* (San Francisco, CA), Sept. 1990.

[4]Coen, P. G., Sobieszczanski-Sobieski, J., and Dollyhigh, S. M., "Preliminary Results from the High-Speed Airframe Integration Research Project," AIAA Paper 92-1004, Feb. 1992.

[5]Giles, G. L., "Equivalent Plate Analysis of Aircraft Wing Box Structures with General Planform Geometry," *Journal of Aircraft*, Vol. 23, No. 11, 1986, pp. 859–864.

[6]Giles, G. L., "Further Generalization of an Equivalent Plate Representation for Aircraft Structural Analysis," *Journal of Aircraft*, Vol. 26, No. 1, 1989, pp. 67–74.

[7]Sobieszczanski-Sobieski, J., "An Integrated Computer Procedure for Sizing Composite Airframe Structures," NASA TP-1300, Feb. 1979.

[8]*DoD/NASA Advanced Composite Design Guide*, Structures/Dynamics Div., Flight Dynamics Lab., Air Force Wright Aeronautical

Lab., Wright-Patterson AFB, Dayton, OH, July 1983.

[9]Kreisselmeier, G., and Steinhauser, R., "Systematic Control Design by Optimizing a Vector Performance Index," *Proceedings of the IFAC Symposium on Computer-Aided Design of Control System* (Zurich, Switzerland), Pergamon Press, Oxford, England, UK, 1980, pp. 113–117.

[10]Barthelemy, J.-F. M., and Riley, M. F., "Improved Multilevel Optimization Approach for the Design of Complex Engineering Systems," *AIAA Journal*, Vol. 23, No. 3, 1988, pp. 353–360.

[11]Carlson, H. W., and Walkey, K. B., "Numerical Methods and a Computer Program for Subsonic and Supersonic Aerodynamic Design and Analysis of Wings with Attainable Thrust Considerations," NASA CR-3808, Aug. 1984.

[12]*Aeroelastic Tailoring of Advanced Composite Structures for Military Aircraft*, Vol. III; also *Modifications and User's Guide for Procedure TSO*, Vol. III, Air Force Flight Dynamics Lab. TR-76-100, Feb. 1978.

[13]Parkinson, A., Balling, R., and Free, J., "OPTDES.BYU A Software System for Optimal Engineering Design, User's Manual," Brigham Young Univ., Provo, UT, 1988.

[14]Fadel, G. M., Riley, M. F., and Barthelemy, J.-F. M., "Two Point Exponential Approximation Method for Structural Optimization," *Structural Optimization*, Vol. 2, 1990, pp. 117–124.

[15]Erikson, W. J., "User Guide: Relational Information Management (RIM)," Boeing Commercial Airplane Co., Rept. D6-IPAD-70023-M, Seattle, WA, 1981.